CHAPTER 7 TRIBOLOGICAL BEHAVIOR OF PMMA/ HAPAG COMPOSITE

This chapter includes the wettability and tribological characterization of the novel hybrid biocomposite of PMMA reinforced with eggshell-derived, silver-doped hydroxyapatite (HAPAg). Tribological response of varying wt% of HAPAg in PMMA are analyzed using a ball-on-disk Tribometer. The coefficient of friction (COF), wear rate, porosity and Vickers microhardness are investigated. The XPS, FTIR, SEM, Stereo zoom microscopy and 3D surface profilometer are used for the characterization. The application of developed biocomposite materials in dental and orthopedic applications are highlighted.

7.1 Results and Discussions

7.1.1 Fourier Transform Infrared Spectroscopy of PMMA-HAPAg composites

The FTIR spectrum of PHA0, PHA2.5, PHA5 and PHA7.5 composite samples, highlighting the presence of functional groups in the PMMA HAp composite, is elaborated in **Fig. 7.2**. As observed, the high intensity vibration peak at 1709 cm^{-1} attributes to stretching band of ester carbonyl group (C=O). The vibration peaks at 744 cm^{-1} and 987 cm^{-1} are attributed to the plane bending of the methyl ($-CH_2$) functional group. Additional peaks of phosphate (PO_4^{3-}) bending mode visible at 578.93 cm^{-1} and sharpening of the broad peak between 1030 cm^{-1} and 1065 cm^{-1} attributed to the asymmetric stretching vibration of phosphate, which confirms the presence of HAp in PMMA [224]. The low intensity peak at 1127.22 cm^{-1} is attributed to asymmetric stretching of the C-O-C bending mode. The two bands at 3024 and 2836 cm^{-1} are ascribed to the C-H stretching vibration of the methyl group. Moreover, a peak at 1385

cm^{-1} corresponds to the C-C-O asymmetric stretching vibration of the methyl carboxyl group [225,226].

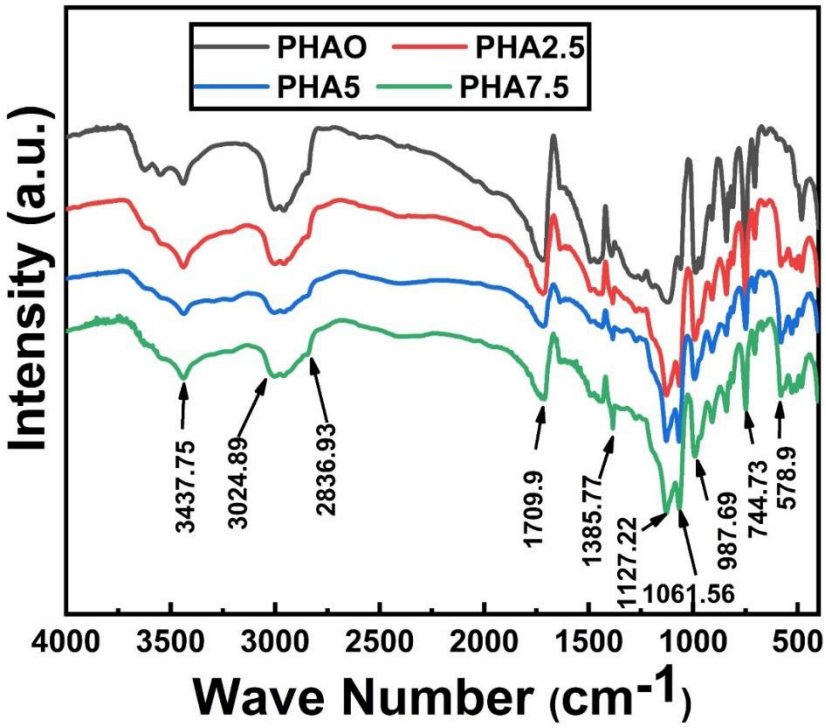

Fig. 7.1. FTIR spectra of (a) PHA0, (b) PHA2.5, (c) PHA5 and (d) PHA7.5.

7.1.2 Elemental analysis using X-ray photoelectron spectroscopy

XPS spectra peaks (using the k-Alpha model by Thermo Fisher Scientific Company) of pure PMMA, i.e., PHA0, are shown in **Fig. 7.2**. The spectra confirm the chemical composition, surface properties and mixing uniformity. The O1s peaks between 528-536 eV bending energy have C=O and C-O functional bending, whereas the C1s curve reflects three peaks reflecting hydrocarbon (C-C, C-H), methoxy group carbon (C-O) and ester (O-C=O) between 282- 290 eV. The high intensity peak in O1s and C1s are at 532.79 eV and 285.21 eV, respectively. Also, the corresponding FWHM values are 3.19 eV and 3.16 eV, and atomic percentages are 30.08 and 69.92 %, which confirms the formation of PMMA polymer as desired [227,228]. The combined XPS spectra (**Fig. 7.3 (a)**), along with the individual elemental spectra of PHA7.5 compositions, are shown in **Fig. 7.3 (b-f).** The presence of silver-doped HAp in PMMA observed on

a 10 nm^2 area (randomly taken) confirms the uniform mixing of silver-doped HAp in PMMA.

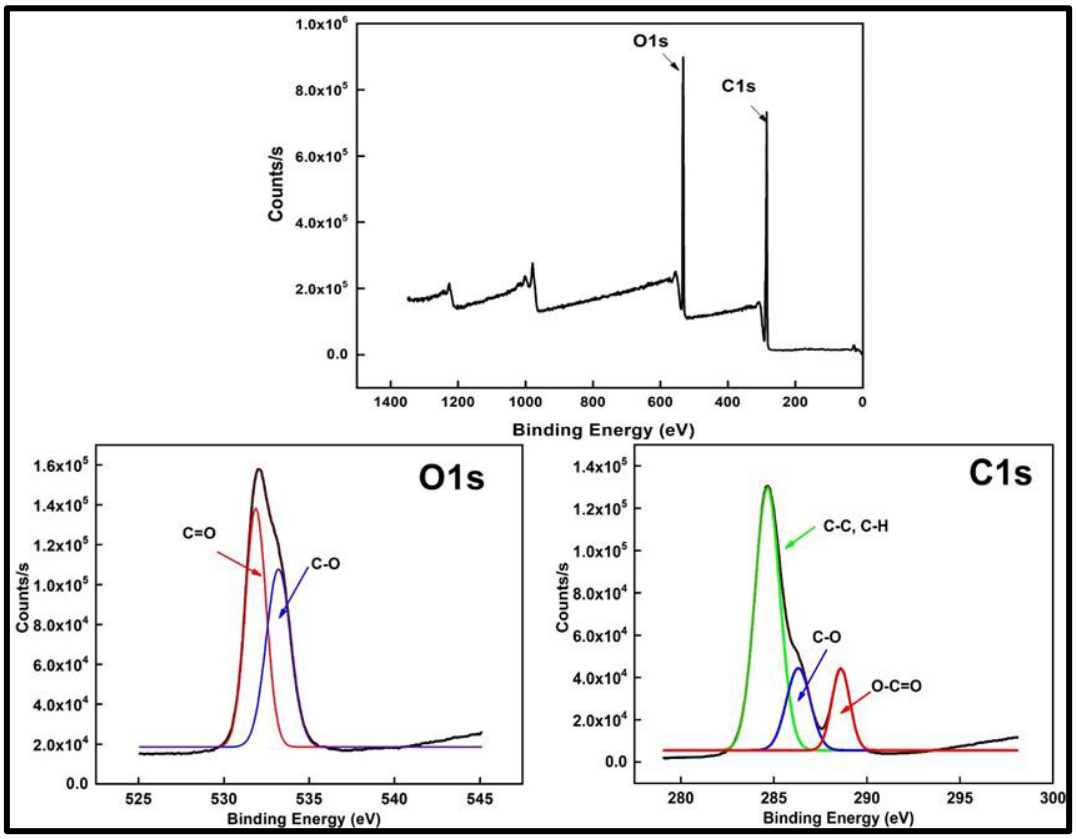

Fig. 7.2. XPS spectra of pure PMMA (PHA0 sample).

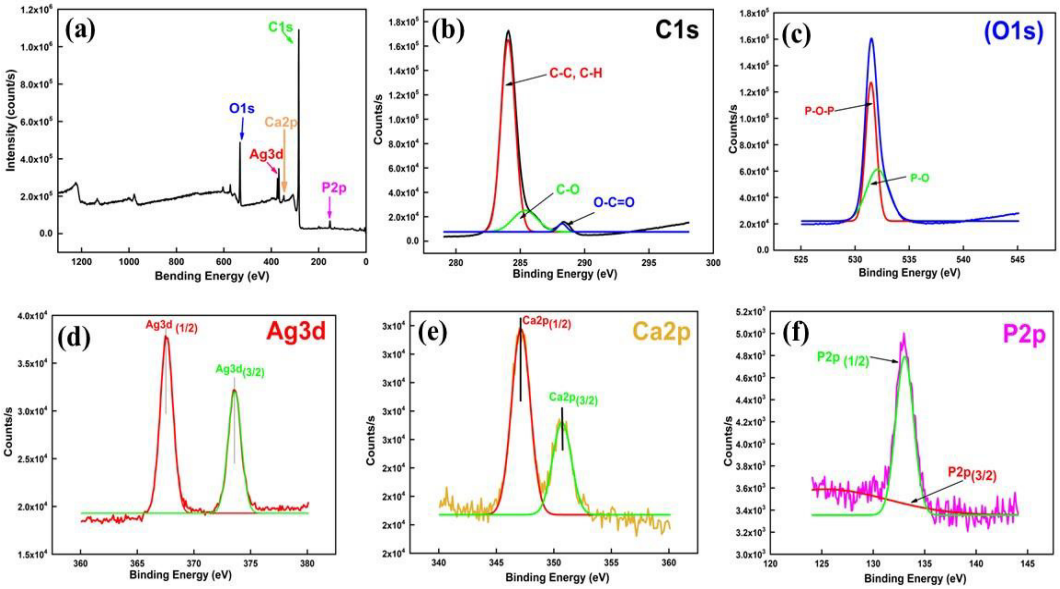

Fig. 7.3. (a) XPS spectra of PMMA reinforced with 7.5wt% silver-doped HAp (PHA7.5), deconvolute peaks for (b) C1s, (c) O1s, (d) Ag3d, (e) Ca2p and (f) P2p.

The deconvolution outputs of PHA7.5 predict a high spectrum peak of Ca2p at 347.06 eV B.E., 2.39 eV FWHM and 0.28 atomic %, C1s at 284.31 eV B.E., 2.81 eV FWHM and 86.53 atomic %, P2p at 133.2 eV B.E., 2.61 eV FWHM and 0.7 atomic %, Ag3d at 367 eV BE 2.42 eV FWHM and 0.56 atomic % and O1s at 532.1 eV B.E., 3.12 eV FWHM and 11.93 atomic % and confirms the bonding between organic-inorganic composition. Among all the elements, Ag3d has a maximum sensitivity factor of 22.131. This outcome is consistent with previously determined standard Ag 3d binding energies for metallic silver [228].

7.1.3 Wettability Analysis of PMMA-HAPAg Composite

The wettability of the composite samples in terms of hydrophilicity and hydrophobicity was determined using water contact angle measurement [214] as shown in **Fig. 7.4.**

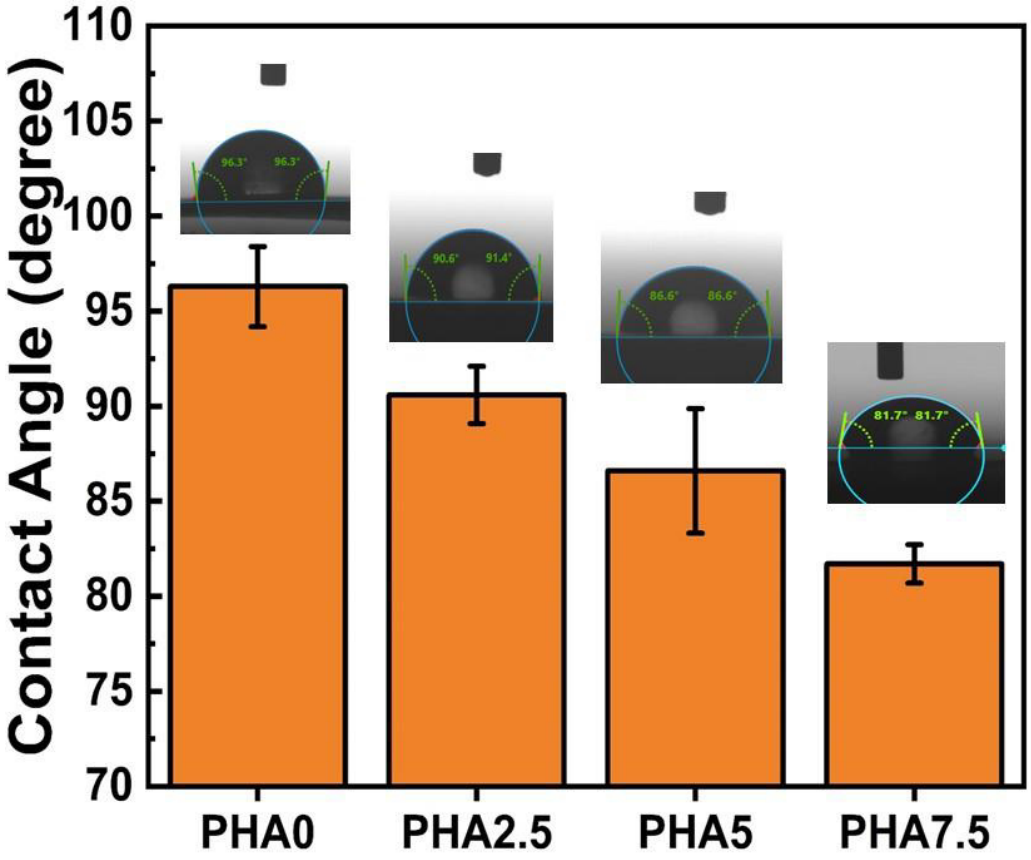

Fig. 7.4. Water contact angle measurement of composite samples.

The cold cure PMMA based composite shows hydrophobic (CA >90^0) characteristics for PHA0 and PHA2.5 with $96.30^0 \pm 2.11^0$ and $90.60^0 \pm 1.50^0$ average contact angles, whereas it shows low-level hydrophilic characteristics for PHA5 ($86.60^0 \pm 3.28^0$) and PHA7.5 ($81.70^0 \pm 1.01^0$) samples. The decrease of 5.91 % in contact angle between PHA0 and PHA2.5 reflects the movement towards hydrophilicity on the addition of HAPAg in PMMA. Also, a 15.16 % change in contact angle is observed between PHA0 and PHA7.5, which shows the composite change from hydrophobic to hydrophilic surface. The decrease in contact angle or increased hydrophilicity is due to the presence of OH ions in the HAp group [229]. The results provide a virtuous sign of biocompatible material devoted to cell growth and proliferation [127]. Also, the composites developed exhibit the minimum water absorption and thickness swelling due to higher contact angle and thus can be best suited for dental applications.

7.1.4 Porosity percentage and Vickers microhardness

The experimental density (ρ_e), theoretical density (ρ_t), porosity (P%) and Vickers microhardness of the prepared samples are tabulated in **Table 7.1**. The maximum relative density of 92.09 % was observed on PHA5 with an experimental density of 1.1314 ± 0.018 g/cm^3. The result reveals that the porosity of the sample decreased with the increase in wt% of HAPAg in PMMA till 5 wt% (PHA5), whereas it shows a minimal increase in the PHA7.5 sample. The increase of 0.505 % porosity without hampering the hardness reflects the occurrence of internal stress concentration [230] that directly impedes the mechanical strength of the PHA7.5 composite[119]. The **Fig. 7.5** shows that the average value of Vickers hardness for PHA0, PHA2.5, PHA5, and PHA7.5 samples are 20.32 ± 0.96, 21.92 ± 0.61, 23.26 ± 0.54, and 24 ± 0.63 HVN, respectively. The magnitude was obtained by applying five indents per sample with 100 g normal load for 10 s dwell time and pitch length 0.2 mm. As the hardness of

HAPAg [231] (31.70 ± 0.989 HVN) particles is higher compared to PMMA (20.32 ± 0.96 HVN), the increase in the concentration of HAPAg contributes significantly to the increase in the hardness [232] of the prepared composite. The 18.11 % increase in Vickers hardness between PHA0 and PHA7.5 governs the 2.86 % decrease in the porosity which reflects the high probability of uniform dispersion of reinforcing HAPAg in PMMA. This improved dispersion leads to better load transfer, resulting in enhanced hardness, and therefore, can also be the reason for the decrease in wear rate and material removal during tribological analysis.

Table 7.1. Theoretical Density, Experimental Density, Porosity % (n=3) and Vickers Microhardness (n=5).

Sample	**Theoretical Density (g/cm^3)**	**Experimental Density (g/cm^3)**	**Porosity (%)**	**Vickers Microhardness (HVN)**
PHA0	1.1900 ± 0.01	1.0732 ± 0.012	9.813 ± 0.13	20.32 ± 0.96
PHA2.5	1.2089 ± 0.01	1.1019 ± 0.022	8.857 ± 0.21	21.92 ± 0.61
PHA5	1.2285 ± 0.01	1.1314 ± 0.018	7.905 ± 0.43	23.26 ± 0.54
PHA7.5	1.2487 ± 0.01	1.1437 ± 0.009	8.410 ± 0.37	24.00 ± 0.63

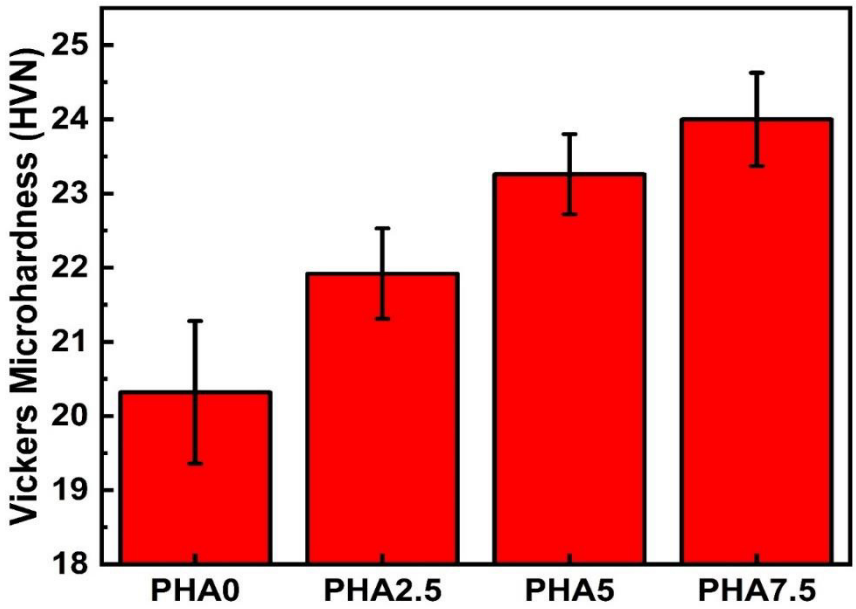

Fig. 7.5. Average Vicker microhardness (HVN) of composite samples.

7.1.5 Effect of normal load on the coefficient of friction

The variation in COF with an increase in sliding distance at varying normal loads (20 N, 40 N and 60 N) and with varying reinforcement of HAPAg in PMMA (0, 2.5, 5 and 7.5%) are shown in **Fig. 7.6 (a-d).** The wear analysis was performed at a constant frequency (14 cps), track length (1.5 mm), sliding time (20 min), temperature 35 ± 2 ^{0}C and 55 ± 1 % relative humidity. As observed, the COF increases rapidly at the beginning of the sliding cycle and then steadily becomes constant during the complete duration.

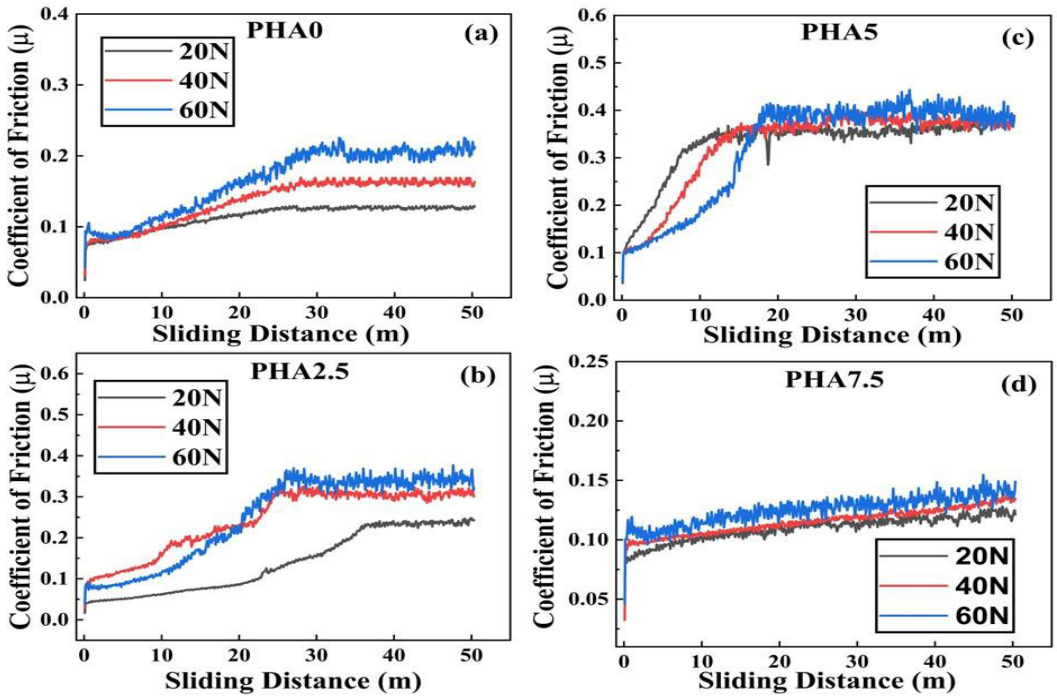

Fig. 7.6. Coefficient of friction v/s Sliding distance at varying load for (a) PHA0, (b) PHA2.5, (c) PHA5 and (d) PHA7.5.

The COF of a composite is diagnosed at this steady state region. **Fig. 7.6 (a)** shows the gradual rise in COF at constant load and frequency for PHA0. The COF increases with the increase in normal load, and at 60N load, it shows 68.75 % and 36.35 % higher COF values than at 20 N and 40 N, respectively. From **Fig. 7.6 (b),** it was observed that the reinforcement of 2.5% HAPAg in PMMA yields higher COF compared to pure PMMA. The value for PHA2.5 increases with the increase in load and shows a 49.25%

increase at 60 N compared to 20 N (COF = 0.224 at 20 N) and 6.26% at 40 N (COF = 0.315 at 40 N). **Fig. 7.6 (c)** shows that the COF for PHA5 at 60 N load steadily rises at the beginning of the sliding and shows the maximum COF (= 0.399). COF at 60 N load is 6.12% and 5.48 % higher than COF at 40 N and 20 N, respectively. COF at a higher sliding distance shows an increasing trend with an increase in normal load for all the samples. The variation in COF with sliding distance at varying loads for PHA7.5 is shown in **Fig. 7.6 (d).** It can be seen that the COF is minimal compared to all other compositions and shows almost constant magnitude with variation in normal load. The minimum COF (0.110) was observed at 20 N load and 7.5 % HAPAg reinforced sample. Several factors like surface hardness, wear mechanism, roughness, synergistic effect, composition, temperature, etc. are responsible for validating the reason behind the variation in COF with load and reinforcement [233]. According to Arnaud et al. [234], the increase in COF with an increase in the normal load can be attributed to an increase in contact area that increases the possibilities of microscopic asperities which further increases interlocking and the frictional force between the mating surfaces. As a result, the COF increases. Also, as seen during the tribo test on PHA7.5, surface smoothing at the contact due to deformation reduces roughness, and forms flattened asperities, and exhibits lower frictional resistance and thus decreases COF [235].

7.1.6 Effect of particle reinforcement on the COF and wear rate

The increase in COF with normal load and HAPAg reinforcement at steady state region was observed in **Fig. 7.7 (a).** However, it was noted that the magnitude of COF for any particular composition has a small change with the variation in load. It was observed that, as the load increases, there is an affinity of a great deformation at the contacting surfaces, which results in the alteration in topography and leads to increase the frictional force which may not significantly affect the coefficient of friction [133]. The

COF at any load increases with the increase in the reinforcement till 5 wt% of HAPAg in PMMA and then decreases suddenly below the COF of pure PMMA in PHA7.5. The increase of 200.8 % (at 20 N), 143.87 % (at 40 N) and 89.1 % (at 60 N) in steady state COF was observed between PHA0 and PHA5 when tested under similar working conditions and parameters. The increase in surface roughness with an addition of HAPAg in PMMA and the interfacial interaction [103] between HAPAg and the contacting surface might enhance the COF with HAPAg reinforcement till 5 wt%. The COF at load 20 N, 40 N and 60 N for PHA0 are 0.125 ± 0.028, 0.155 ± 0.048 and 0.212 ± 0.071; for PHA2.5 are 0.22432 ± 0.119, 0.31509 ± 0.097 and 0.33482 ± 0.14, for PHA5 are 0.37619 ± 0.07, 0.37847 ± 0.09 and 0.39922 ± 0.133 and for PHA7.5 are 0.11034 ± 0.011, 0.12472 ± 0.025 and 0.1275 ± 0.015, respectively. The sudden decrease in the COF at PHA7.5 sample was attributed to the contact mechanism between the mating surfaces indicating surface smoothening through running-in mechanism and formation of flattened asperities on the wear track at PHA7.5. Also, the reduction in the actual contact area was visible which resulted in a decrease in frictional resistance and the COF [236].

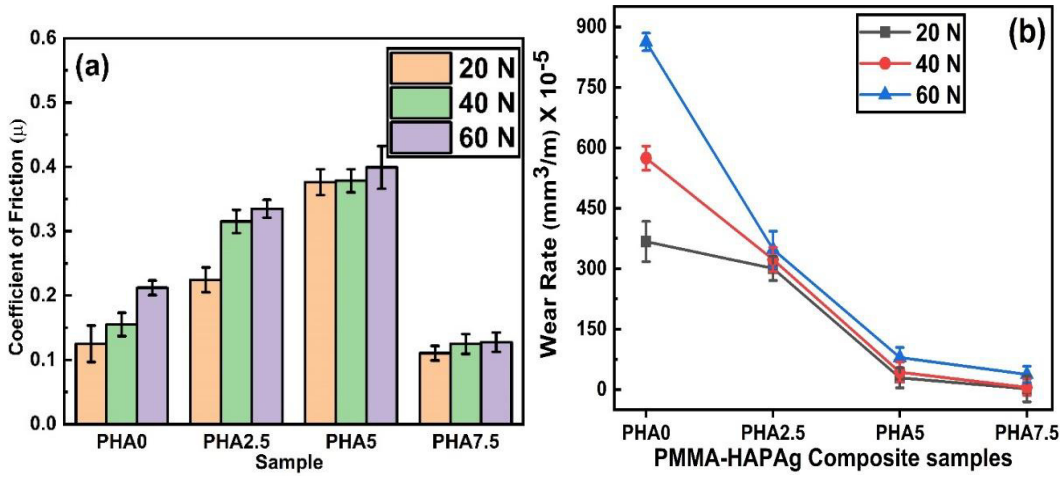

Fig. 7.7. Variation in (a) COF and (b) wear rate with varying wt % of silver-doped HAp in PMMA at different normal loads.

The effect of load and particulate reinforcement on the wear rate of the composite samples at constant speed and time is shown in **Fig. 7.7 (b).** The wear rate for HAPAg-reinforced composite materials gradually decreases with an increase in reinforcement. However, a sudden decrease in the wear rate was observed in the PHA7.5 composite samples, which can be due to the increase in surface hardness and adhesion strength with an increase in reinforcement wt% [237]. The graph in **Fig. 7.7 (b)** shows the minimal variation in the wear rate with load for the HAPAg reinforced composites (PHA2.5. PHA5 and PHA7.5) whereas in case of PHA0 (pure PMMA composite), approximately 134.71% rise in wear rate was observed between 20 N and 60 N load. The results are correlated with the earlier reported work by Yadav et al. [134]. The abrupt decline in the wear rate for PHA7.5 was attributed to the improved bonding adhesion that distributes the applied load over the wide surface area and thus decreases pressure at the contact point. The highest wear rate was observed for PHA0 (i.e., $862.42*10^{-5}$ mm^3/m) at 60 N. However, the wear rate decreased by 52.2% on increasing the wt % of HAPAg from 5 to 7.5 % at a normal load of 60 N. Apart from PMMA and HAPAg, several other biocompatible polymer-based composites are being fabricated and tribologically characterized in the form of bulk and coatings for oral and dental implant applications. Pedroso et al. [238] performed the comparative tribological analysis between PEEK (polyetheretherketone) and PEKK (polyetherketoneketone) polymers and revealed that the PEKK-based coating shows negligible wear while sliding for approximately 1500 m with 20 N load at 0.1 m/s speed whereas PEEK shows $105*10^{-5}$ mm^3/m wear with similar COF (0.11). The wear rate of PEEK lies between PHA2.5 and PHA5. Morales et al. [239] determined the specific wear rate of biocomposite with carbonated HAp reinforcement in PMMA in the range of $3.75*10^{-5}$ to $8.13*10^{-5}$ mm^3/Nm at low loads (i.e. 2-10 N) which are close

to specific wear rate of PHA2.5 between 20- 40 N normal load. Also, titanium- Copper (Ti–5Cu) alloy for dental applications, characterized by Pandey et al. [235] indicates the high hardness (458 ± 16.32 HVN) and very low wear rate ($12.88*10^{-8}$ mm^3/m) at 20 N load under SBF medium. Rahmani et al. [240] evaluated the wear rate of glass fibre (GFR), carbon fibre (CFR) and Kevlar fibre (KFR) reinforced polymer composite and reported that the wear rate of GFR, CFR and KFR tested at 0.1 m/s scratch speed with 10 N normal load for 300 m sliding distance in the dry state were 7.6, 6 and 9.3 mg/m, respectively which is comparatively higher than the wear rate of PHA7.5 scratched at 20 N normal load. Also, it can be concluded that the wear rate increases as the normal load increases while it shows a decreasing trend with the percentage of HAPAg reinforcement for all compositions due to the uniform compositional characteristics of the prepared samples which concludes the dependency of wear directly with respect to contact pressure [241].

7.1.7 Preliminary visual inspection of worn surfaces

The initial visual inspection of the worn track was analyzed using a Zeiss stereo-zoom microscope. The sliding direction, worn topology and the influence of varying load on the composite sample are shown in **Fig. 7.8 (a-l).** The influence of normal load and the HAPAg reinforcement during the wear analysis was visualized through the microscopic images. **Fig. 7.8 (a-c)** shows wear on the PHA0 sample at 20 N, 40 N and 60 N loads, respectively. Sliding directions for the tribological analysis are marked on the images. The decrease in wear scars at PHA7.5 (**Fig. 7.8 (j-l)**)were observed in the microscopy, which could be due to the increase in surface hardness and the variation in wear mechanisms with change in the composition of the composites. Further morphology was analyzed using SEM images. The depth and the width of the worn surface along the central transverse direction are plotted using a surface 3D

profilometer, as shown in **Fig. 7.8 (a-l).** The 2D profile of the worn surface along its central position is plotted for wear rate analysis. The surface area at the central track and FWHM values are calculated using origin software and marked above each curve. The worn area is directly proportional to the wear rate. The maximum depth value, FWHM, and transverse area at varying loads are tabulated in **Table 7.2.**

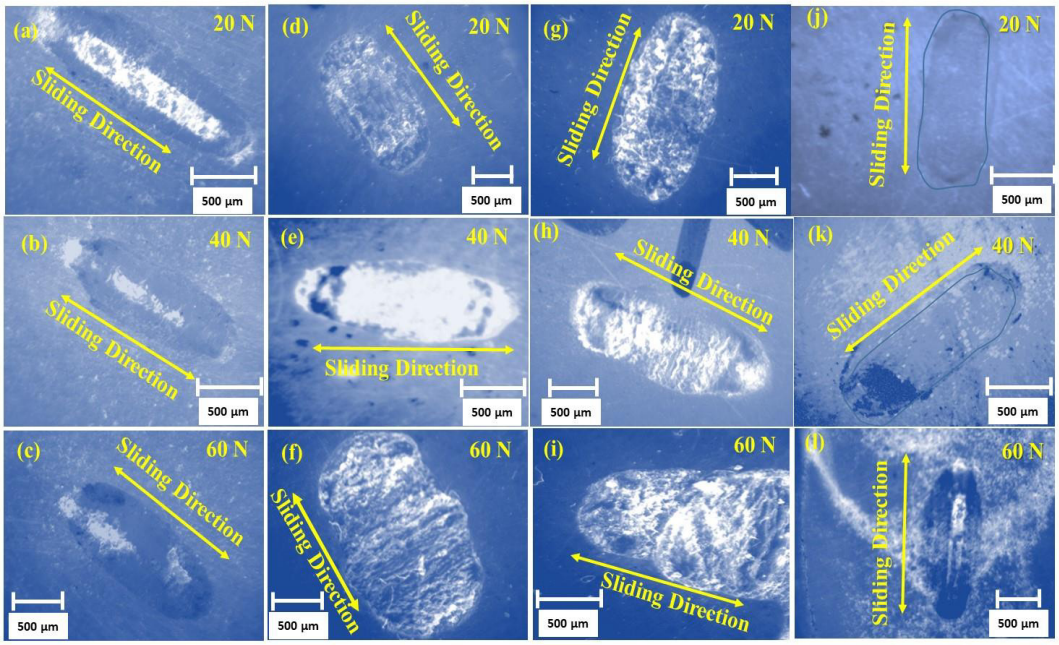

Fig. 7.8. Stereo zoom images of worn track for PHA0 (a, b, c), PHA2.5 (d, e, f), PHA5.0 (g, h, i) and PHA7.5 (j, k, l) at 20 N, 40 N and 60 N.

7.1.8 Transverse wear area analysis using a profilometer

The depth and the width of the worn surface along the central transverse direction were plotted using a surface 3D profilometer as shown in **Fig. 7.9 (a-l)**. The 2D profile of the worn surface along its central position is plotted for wear rate analysis. The surface area at the central track and FWHM values listed in **Table 7.2.** are evaluated using origin software and marked above each curve.

Table 7.2. Transverse wear area, FWHM, wear depth, volume loss and average wear rate of the worn surface.

Sample	Load (N)	Area (μm²)	FWHM (μm)	Average depth value (μm)	Volume Loss (mm^3)	Average Wear Rate (mm^3/m) x 10^{-5}	Specific Wear Rate (mm^3/Nm) x 10^{-5}
PHA0	20	95924.69 ±10	1338.53	51.64 ± 0.10	0.1851 ± 0.05	367.44 ± 0.001	18.37 ± 0.0001
	40	144876.85 ±10	1481.49	68.24 ± 0.23	0.2893 ± 0.01	574.14 ± 0.001	14.35 ± 0.0001
	60	212984.20 ±10	1635.23	86.32 ± 0.07	0.4346 ± 0.02	862.42 ± 0.001	14.37 ± 0.0001
PHA2.5	20	79322.89 ±10	1260.39	45.90 ± 0.15	0.1516 ± 0.00	300.84 ± 0.001	15.04 ± 0.0001
	40	85844.53	1199.58	46.83 ± 0.09	0.1627 ± 0.04	322.91 ± 0.001	8.07 ± 0.0001
	60	92297.94 ±10	1287.91	48.86 ± 0.40	0.1753 ± 0.01	348.02 ± 0.001	5.80 ± 0.0001
PHA5	20	8439.34 ±10	155.91	12.05 ± 0.15	0.0149 ± 0.01	29.59 ± 0.001	1.48 ± 0.0001
	40	12641.56 ±10	493.32	13.62 ± 0.11	0.0218 ± 0.02	43.34 ± 0.001	1.08 ± 0.0001
	60	23085.27 ±10	557.76	18.95 ± 0.14	0.0402 ± 0.03	79.76 ± 0.001	1.33 ± 0.0001
PHA7.5	20	734.39 ±10	401.29	00.92 ± 0.18	0.0011 ± 0.01	2.21 ± 0.001	0.11 ± 0.0001
	40	1944.32 ±10	1375.78	01.36 ± 0.23	0.0029 ± 0.01	5.84 ± 0.001	0.14 ± 0.0001
	60	11557.86 ±10	673.82	10.99 ± 0.09	0.0192 ± 0.00	38.12 ± 0.001	0.63 ± 0.0001

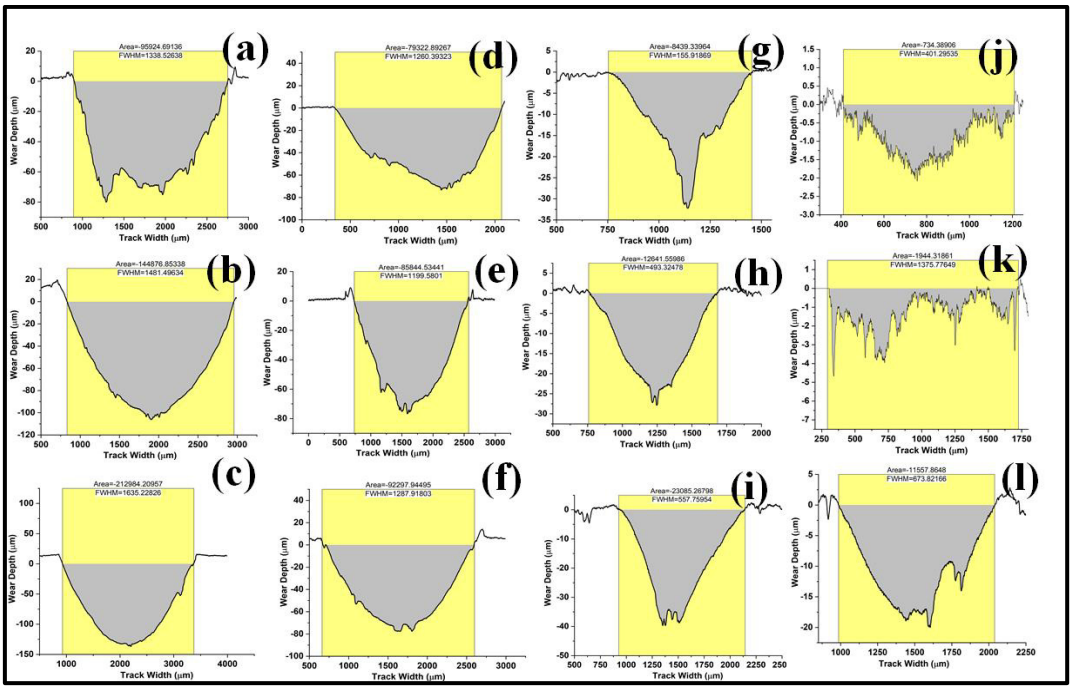

Fig. 7.9. Worn area and maximum depth measurement along transverse direction by surface profilometer for PHA0 (a, b, c), PHA2.5 (d, e, f), PHA5 (g, h, i) and PHA7.5 (j, k, l) at 20 N, 40 N and 60 N normal load.

The worn area is directly proportional to the wear rate [242]. As observed, the worn area at the center of the track length shows an increase in magnitude with the increase in applied normal load. The maximum wear area was evaluated when the load of 60 N was applied at 14 cps frequency on the pure PMMA sample for a 50.4 m sliding distance. The wear created 86.32 µm average deep groove and a 132.4 µm maximum groove at the center (**Fig. 7.9 (c)**). The average depth values, FWHM, transverse area at varying loads and constant frequency for various composite samples are tabulated in **Table 7.2**. Interestingly, the 3D- profilometer also helps to evaluate the maximum wear rate of the worn surfaces [235,243].

7.1.9 Morphological analysis of worn surface

In the schematic illustration of the wear mechanism shown in **Fig. 7.10 (a-d)**, distinct patterns emerge reflecting the tribological mechanism of the composite with varying loads (20, 40 and 60 N) and reinforcement concentrations (0, 2.5, 5 and 7.5 wt%).

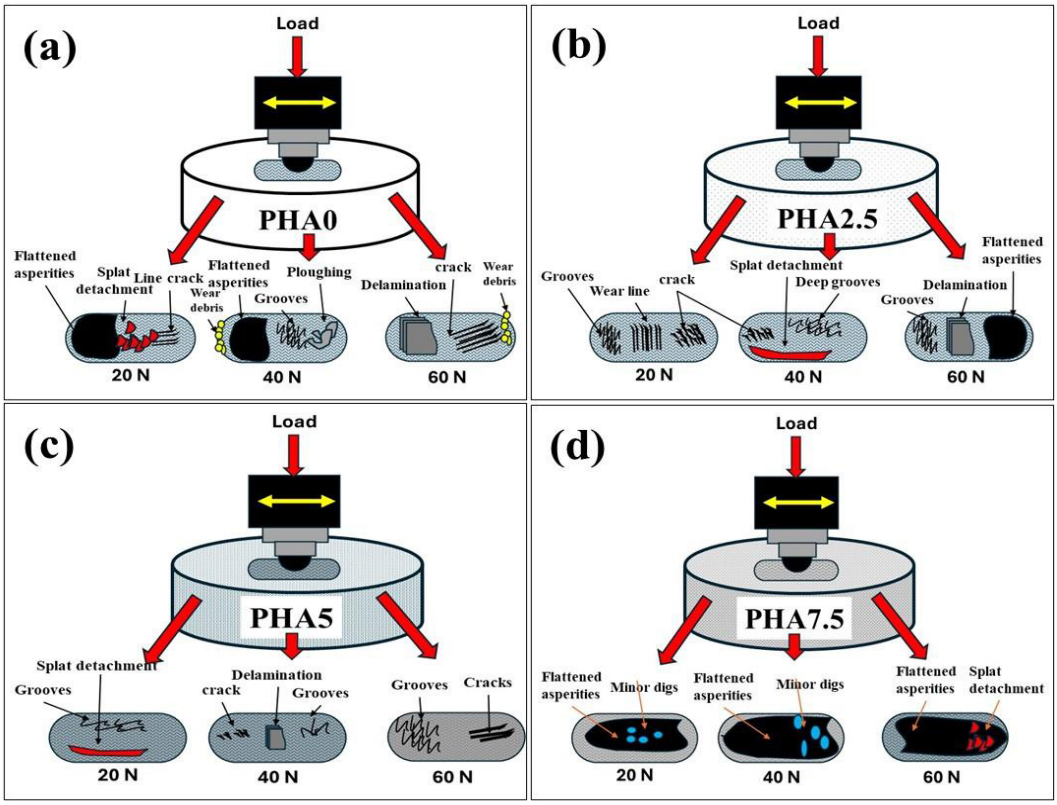

Fig. 7.10. Schematic illustration of the wear mechanism during the tribological analysis of (a) PHA0, (b) PHA2.5, (c) PHA5 and (d) PHA7.5.

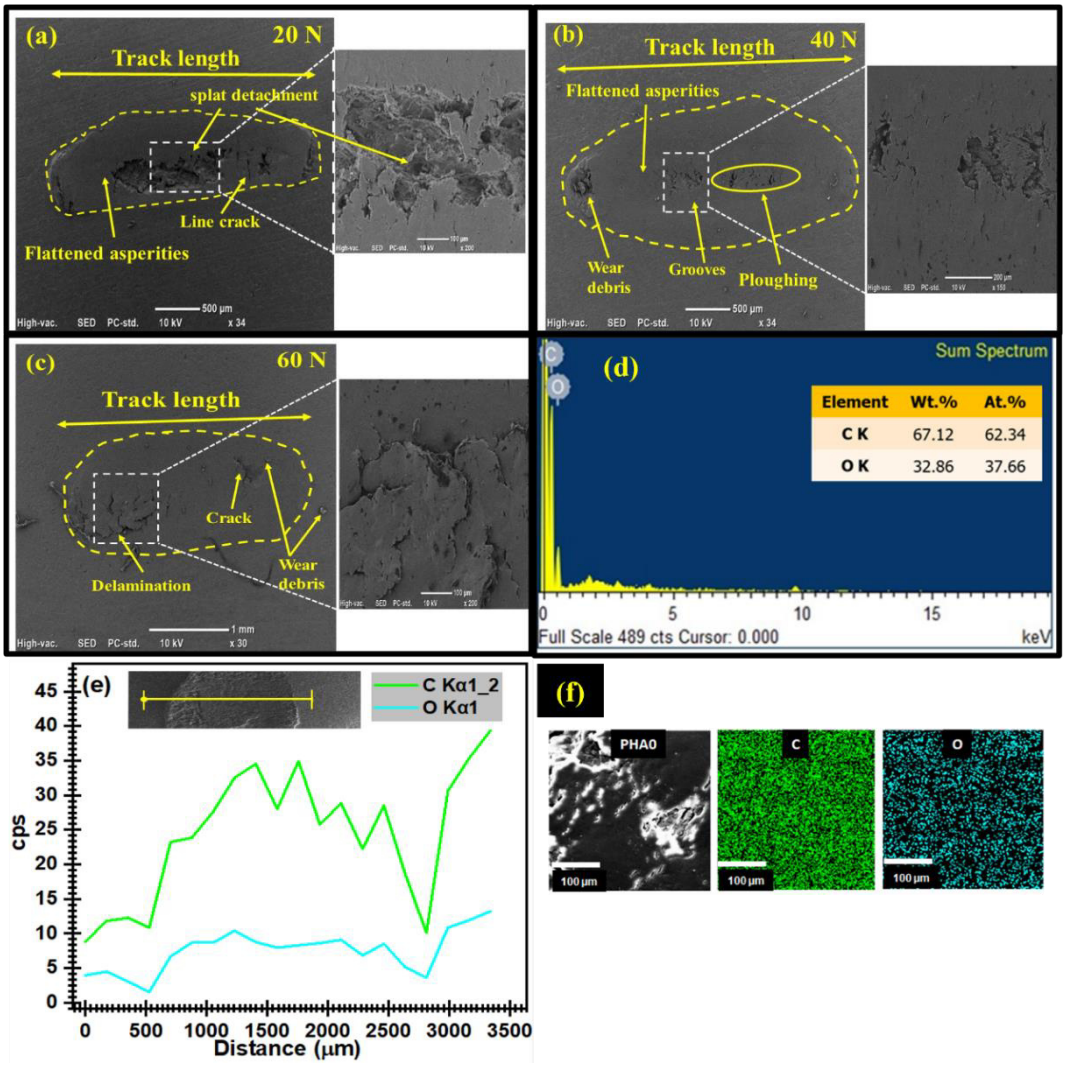

Fig. 7.11. SEM micrographs of worn surface of PHA0 at (a) 20 N, (b) 40 N and (c) 60 N Normal Load, (d) point EDS, (e) line EDS at 60 N and (f) elemental mapping.

At lower concentration, the wear is maximum due to the extreme abrasive and adhesive wear mechanism which leads to the inculcation of delamination, cracks, grooves and splat detachment. The dependency of COF and amount of wear was governed and correlated with the micrographs, providing valuable insights into the complex interplay between reinforcement content and wear mechanisms, guiding further investigation and optimization of HAPAg reinforced PMMA composite.

The morphologies of the worn-out surface of the composite disc offer clues to the sliding wear mechanism against the applied normal load and percentage of particle reinforcement. The morphological analysis reveals the nature of wear on the

specimens. **Figs. 7.11-7.15** shows the wear track morphology of the tested samples. As observed, all the tested samples show mainly the abrasive or erosive type of wear mechanism [234].

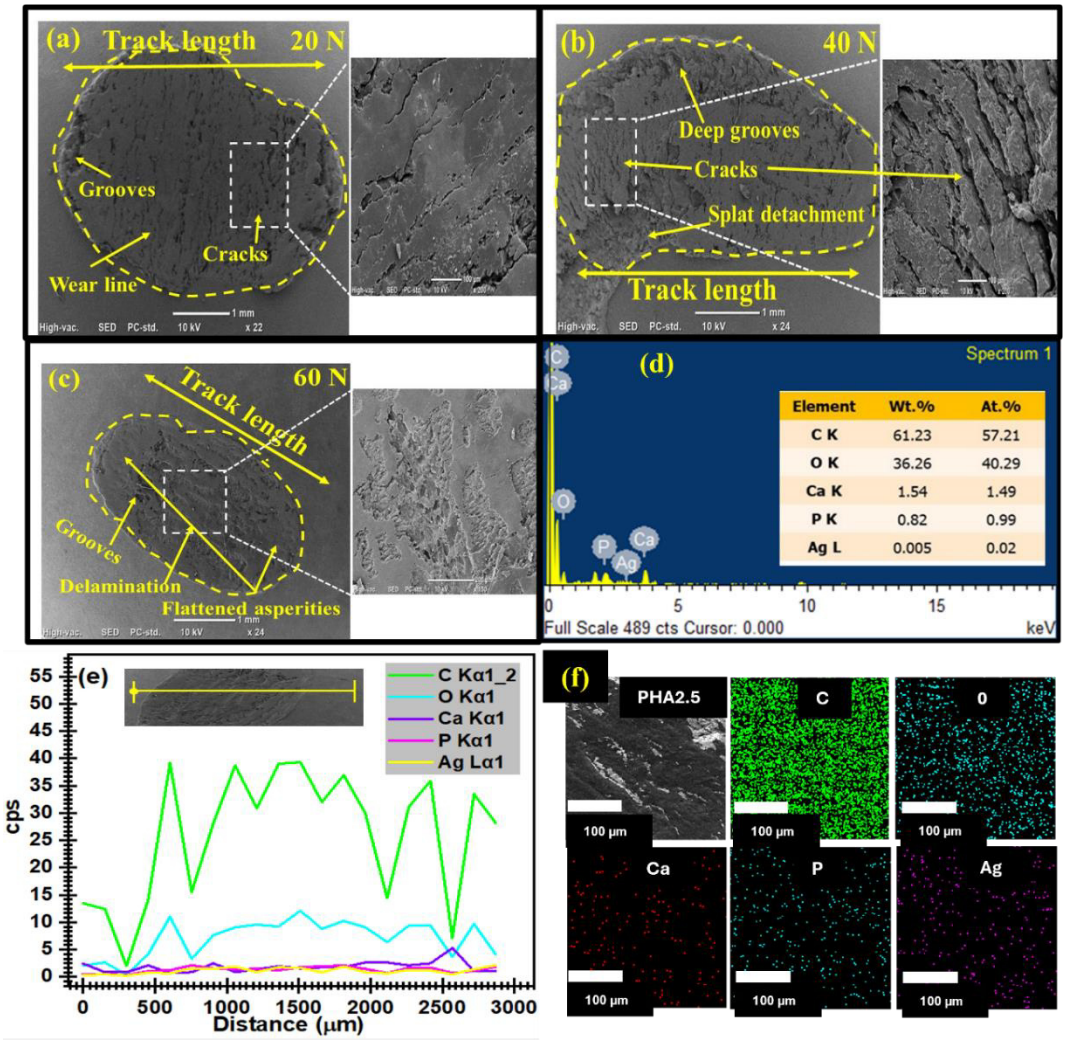

Fig. 7.12. SEM image of worn surface of PHA2.5 at (a) 20 N, (b) 40 N and (c) 60 N Normal Load, (d) point EDS, (e) line EDS at 60 N and (f) elemental mapping.

The morphology of the worn surface of the PHA0 composite sample at varying loads is shown in **Fig. 7.11 (a-c)**. The splat detachment, flattened asperities and line cracks were observed on the wear track at 20 N, which signifies an abrasive wear mechanism [244], as shown in **Fig. 7.11 (a).** The wear at 40 N load shows the increased area in the track length with debris, minor grooves and ploughing, as shown in **Fig. 7.11 (b).** The delamination and the cracks on the wear surface are observed when a load of 60 N is applied to the PHA0 composite. The surface roughening in PMMA-based composite

increases friction at higher loads [245]. The deformation is visible in **Fig. 7.11 (a).** The spreading of debris between the surface of sliding is considered responsible for the decrease in specific wear rate between the contacting surfaces at 60 N load [246]. The **Fig. 7.11 (d-f)** highlights the point, line and area EDS, respectively of PHA0 which confirms the material composition and uniformity.

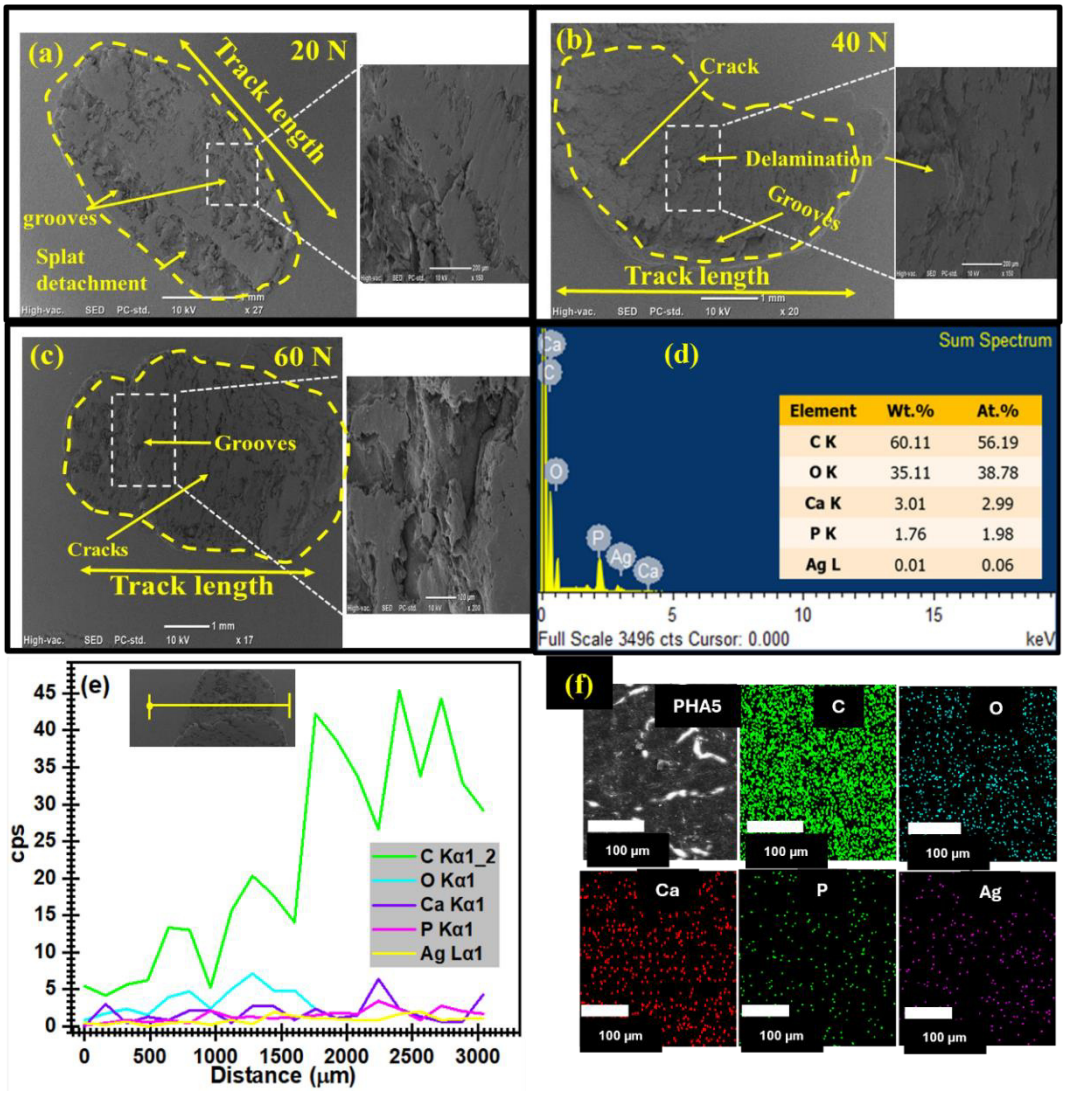

Fig. 7.13. SEM image of worn surface of PHA5 at (a) 20 N, (b) 40 N and (c) 60 N Normal Load, (d) point EDS, (e) line EDS at 60 N and (f) elemental mapping.

The SEM micrographs of the worn surface along the track length for PHA2.5 composites at varying loads are shown in **Fig. 7.12 (a-c)**. Reinforcement of HAPAg in PMMA increases the friction, and the wavey lines, parallel cracks and deep grooves are formed during the wear when a 20 N load is applied (**Fig. 7.12 (a)**) on the sample

that shows an abrasive type wear mechanism [247]. The deep grooves, splat detachment and parallel cracks are observed in **Fig. 7.12 (b)**, where 40 N normal load was applied between the contacting surfaces. The deep grooves, delamination and flattened asperities at 60 N load on the surface along the track length with particle reinforcement reflect its wear characteristics (**Fig. 7.12 (c)).**

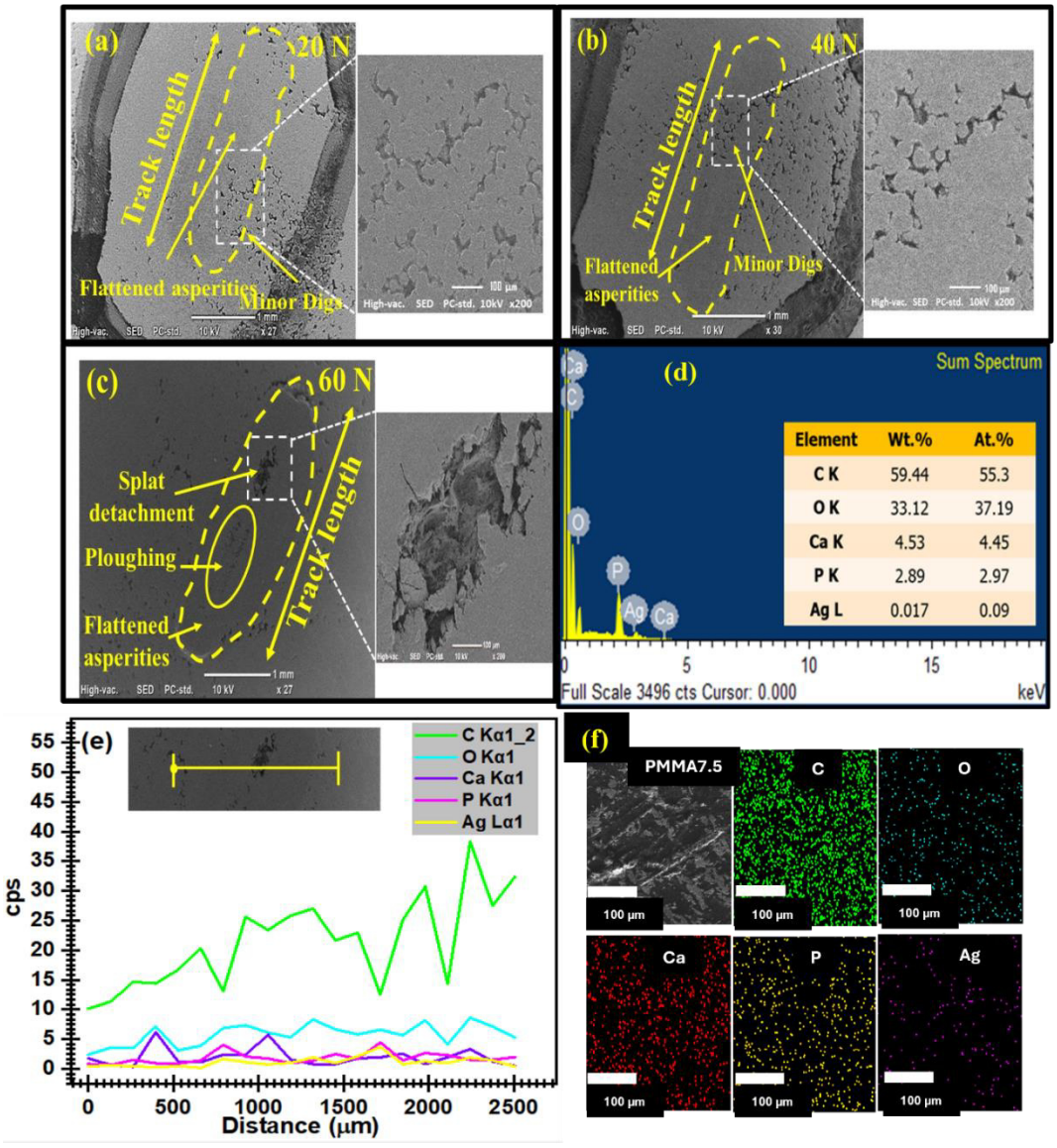

Fig. 7.14. SEM image of worn surface of PHA7.5 at (a) 20 N, (b) 40 N and (c) 60 N Normal Load, (d) point EDS, (e) line EDS at 60 N and (f) elemental mapping.

The increase in the surface area at higher loads decreases the friction resistance, and thus, an increase in COF occurs at higher loads. The **Fig. 7.12 (d-f)** highlights the point, line scar and area EDS, respectively of PHA2.5 after the wear test, and the output

reveals the uniform dispersion of HAPAg in PMMA that results in the increase in surface hardness of the composite sample.

The surface morphology of the PHA5 at various normal loads during the wear test are shown in **Fig. 7.13 (a-c)**. The wear surface at 20 N load as shown in **Fig. 7.13 (a)**, results in deep grooves and splat detachment with high material removal and thus has high COF similar to the erosive wear mechanism [248]. The **Fig. 7.13 (b)** shows the worn surface with line cracks, grooves, and delamination when a normal load of 40 N is applied to the PHA5 composite. A large amount of debris has accumulated near the track surface, and the wear during the 60 N load forms deep grooves and line cracks, as shown in **Fig. 7.13 (c)**. The plastic deformation provides an interlocking between the contacting surfaces and thus decreases the specific wear rate at higher loads [249]. The point, line and area EDS of PHA5 are shown in **Fig. 7.13 (d-f)**. The intensity of radiations in line graph (**Fig. 7.13 (e)**) and the results of elemental mapping (**Fig. 7.13 (f)**) concludes the stable mixing of HAPAg in PMMA.

In PHA7.5 composite samples, a rapid decrease in COF was observed, and the surface morphology shown in **Fig. 7.14 (a-c)** shows a minor deformation in the track length. The PHA7.5 composite shows appreciable wear resistance when 7.5 wt% of HAPAg is reinforced in PMMA. **Figure. 7.14 (d-f)** shows the uniform dispersion of HAPAg in PMMA that provides improved adhesion and bonding between PMMA and HAPAg. High surface hardness was observed with negligible wear rate at 20 N and 40 N loads. **Figure. 7.14 (a)** shows minor scratches and flattened asperities on the surface of the composite when a 20 N load at 14 cps is applied for the wear analysis. The results are more promising at higher loads as minor digs and deformation are observed during

tribological tests with 40 N and 60 N normal loads, as shown in **Fig. 7.14 (b) and (c).** However, small splat detachment wear was observed when a high load of 60 N was applied to the PHA7.5 composite. The decrease in wear rate with the increase in reinforcement at higher reinforcement concentration can be due to the improved surface hardness that provides minimum wear and COF. Also, the rise in adhesion at higher loads increases the attractive force and reduces relative motion between the contacting surfaces, thus reducing COF [250].